

# Shear-induced crystallization of a dense rapid granular flow: hydrodynamics beyond the melting point?

Evgeniy Khain<sup>1</sup> and Baruch Meerson<sup>2</sup>

<sup>1</sup>*Department of Physics and Michigan Center for Theoretical Physics,  
The University of Michigan, Ann Arbor, Michigan 48109 and*

<sup>2</sup>*Racah Institute of Physics, Hebrew University of Jerusalem, Jerusalem 91904, Israel*

We investigate shear-induced crystallization in a very dense flow of mono-disperse inelastic hard spheres. We consider a steady plane Couette flow under constant pressure and neglect gravity. We assume that the granular density is greater than the melting point of the equilibrium phase diagram of elastic hard spheres. We employ a Navier-Stokes hydrodynamics with constitutive relations all of which (except the shear viscosity) diverge at the crystal packing density, while the shear viscosity diverges at a *smaller* density. The phase diagram of the steady flow is described by three parameters: an effective Mach number, a scaled energy loss parameter, and an integer number  $m$ : the number of half-oscillations in a mechanical analogy that appears in this problem. In a steady shear flow the viscous heating is balanced by energy dissipation via inelastic collisions. This balance can have different forms, producing either a uniform shear flow or a variety of more complicated, nonlinear density, velocity and temperature profiles. In particular, the model predicts a variety of multi-layer two-phase steady shear flows with sharp interphase boundaries. Such a flow may include a few zero-shear (solid-like) layers, each of which moving as a whole, separated by fluid-like regions. As we are dealing with a hard sphere model, the granulate is fluidized within the “solid” layers: the granular temperature is non-zero there, and there is energy flow through the boundaries of the “solid” layers. A linear stability analysis of the uniform steady shear flow is performed, and a plausible bifurcation diagram of the system, for a fixed  $m$ , is suggested. The problem of selection of  $m$  remains open.

PACS numbers: 45.70.Mg, 83.50.Ax

## I. INTRODUCTION

In spite of extensive experimental and theoretical studies of dense granular flows, a theoretical description of these flows remains challenging [1]. Multi-particle contacts and friction, intrinsic in slow dense flows, invalidate the kinetic theory [2, 3]. Furthermore, even rapid dense flows (that is, flows dominated by binary collisions) present significant difficulties for analysis. Dilute and moderately dense flows of mono-disperse inelastic hard sphere fluids are describable, for not too high inelasticity of collisions, by Navier-Stokes hydrodynamics [3], which can be derived in a systematic way from the kinetic theory: a one-particle kinetic equation properly generalized to account for inelastic collisions [2, 3]. Hydrodynamic equations, that is conservation laws for the mass and momentum of the granulate, and a balance equation for the energy, may still be valid, for a hard sphere fluid, at higher densities, after the disorder-order transition occurs. However, the respective constitutive relations are not derivable from a kinetic equation anymore.

In this work we attempt to address this difficulty and suggest a possible hydrodynamic description of a sheared rapid granular flow that exhibits crystallization. Shear-induced ordering in a dense granular medium has attracted much recent attention. It was investigated experimentally (usually for slow flows) by many groups [4, 5, 6]. The crystallization dynamics in inelastic hard sphere fluids has been also extensively studied in MD simulations [7, 8]. In this work we will be dealing with an idealized model of inelastic particle collisions charac-

terized by a constant coefficient of normal restitution  $r$ , and focus on a plane shear flow.

The present work is a next step in a series of recent attempts of extending granular hydrodynamics of inelastic hard sphere fluids to high densities [9, 10, 11]. Grossman *et al.* [9] investigated a prototypical system of inelastic hard disks at zero gravity, placed in a two-dimensional rectangular box, one wall of which serving as a “thermal” wall. Grossman *et al.* suggested an equation of state, granular heat conductivity and inelastic energy loss rate which interpolated between the dilute limit and the close vicinity of the hexagonal close packing, where free-volume arguments are available. The density profiles, obtained by solving the hydrostatic equations numerically, were in good agreement with the results of MD simulations [9].

Meerson *et al.* [11] considered a similar two-dimensional granular system, but with gravity. The system was driven from below by a “thermal” base. Employing the constitutive relations suggested by Grossman *et al.* [9], Meerson and coworkers found steady-state density and temperature profiles and observed good agreement with MD simulations, including the region of the “levitating cluster”, where the density is very close to that of hexagonal close packing [11].

Bocquet *et al.* [10] employed hydrodynamic equations to model a granular shear flow where the density approached the random close packing density. They also compared their theory with experiment in a circular Couette flow [10]. As a shear flow was present, Bocquet and coworkers had to specify, in addition to the rest of the

constitutive relations, the coefficient of shear viscosity. In experiment the granular temperature had been found to decrease more slowly, with an increase of the distance from the shear surface, than the velocity. To account for this finding, Bocquet *et al.* assumed that the shear viscosity diverges more rapidly, at random close packing, than the rest of the transport coefficients.

We employ in this work Navier-Stokes granular hydrodynamics for a description of a steady crystallized shear flow of an assembly of mono-disperse inelastic hard spheres under constant pressure. Our approach is similar to that taken by Bocquet *et al.* [10], with two important differences. First, we focus on the ordered crystalline phase which ends at the crystal (hexagonal or face-centered cubic) close packing density  $\phi_{fcc}$ , whereas Bocquet *et al.* considered the metastable disordered phase which ends at the random close packing density  $\phi_{rcp}$ . Second, we assume that the shear viscosity diverges at a *smaller* density than the rest of transport coefficients, see below. This assumption brings about the possibility of a two-phase steady flow. In general, a granular shear flow reaches a steady state when the viscous heating makes up for the energy dissipation via inelastic collisions. As we show here, this balance can be achieved in different ways, producing either a uniform shear flow, or a variety of flows with nonlinear density, velocity and temperature profiles. Working in the range of densities beyond the melting point, we determine the phase diagram of dense steady flows in terms of three parameters: an effective Mach number, a scaled energy loss parameter, and an integer number  $m$ : the number of half-oscillations in a mechanical analogy that appears in this problem. There are regions on this phase diagram where two or more different steady flow solutions are possible for the same values of the parameters. To get an additional insight, we perform a linear stability analysis of the uniform steady shear flow. Based on these results, we suggest a plausible bifurcation diagram of the system which, in some region of the parameter space, describes bistability and hysteresis.

The rest of the paper is organized as follows. In Sec. 2 we introduce our shear-induced crystallization scenario and the governing hydrodynamic equations and constitutive relations. Section 3 describes our model of a zero-gravity constant-pressure shear flow and focuses on the analysis of a crystallized steady shear flow in different regimes. Section 4 presents a linear stability analysis of the uniform shear flow solution and suggests a plausible bifurcation diagram of the system. Details of the linear stability analysis are presented in the Appendix. Section 5 includes a brief discussion and summary of our results.

## II. PRESSURE-DENSITY DIAGRAM AND HYDRODYNAMIC EQUATIONS

Figure 1 depicts, in the coordinates “volume fraction - pressure”, the phase diagram of a homogeneous macro-

scopic system of *elastic* hard spheres [12]. The volume fraction  $\phi = (\pi/6)d^3n$  (where  $n$  is the particle number density, and  $d$  is the particle diameter) changes from zero to  $\phi_{fcc} = \sqrt{2}\pi/6 \simeq 0.74$ , the density of crystal (either hexagonal, or face-centered cubic) close packing, the densest possible packing of spheres in three dimensions. The phase diagram includes four branches. The disordered, or gas/liquid branch starts at  $\phi = 0$  and continues until the freezing point that occurs at  $\phi \simeq 0.494$ . Then this branch splits into two branches. The horizontal (constant pressure) branch describes coexistence of the disordered and ordered phases. It starts at the freezing point and ends at the melting point at  $\phi \simeq 0.545$ . At larger volume fractions the system is in the ordered crystalline phase that ends at the density of the crystal close packing  $\phi_{fcc}$ . The last branch is a *metastable* extension of the gas/fluid branch. It starts at the freezing point and ends at random close packing at  $\phi_{rcp} \simeq 0.64$ . Clearly, each branch is described by a separate equation of state.

The phase diagram, presented in Fig. 1, appears in the context of a homogeneous system in either equilibrium, or a metastable state. Granular systems are usually inhomogeneous and, no less important, they are intrinsically far from equilibrium, due to inelastic collisions between particles. We will deal, however, with a small inelasticity of particle collisions and, in the spirit of kinetic theory [2, 3], assume that the system is everywhere close to *local* thermodynamic equilibrium, so the phase diagram (and the constitutive relations presented below) are valid locally. Let the fluid density be sufficiently large, so that the volume fraction is everywhere above the melting point. There are two possible phases here. One of them is the disordered phase (the the metastable branch in Fig. 1), the other one is the crystallized phase. Each of the two phases, disordered and ordered, can have inhomogeneous temperature and density profiles, without violating the constancy of the pressure. Furthermore, domains of disordered phase can in principle coexist with domains of the ordered phases (again, without violating the constancy of the pressure). Shear-induced crystallization apparently represents a (non-equilibrium) phase transition, so that the metastable disordered branch gives way, everywhere, to the stable ordered branch.

This work addresses very dense flows, where the volume fraction is close to that of the crystalline close packing,  $\phi_{fcc} - \phi \ll \phi_{fcc}$ . We assume that the ordered crystalline branch of the phase diagram (see Fig. 1) has already won in the competition with the disordered branch. To describe a flow in this phase, one needs hydrodynamic equations. These represent the mass conservation

$$\frac{dn}{dt} + n \nabla \cdot \mathbf{v} = 0, \quad (1)$$

the momentum conservation

$$n \frac{d\mathbf{v}}{dt} = \nabla \cdot \mathbf{P} + n \mathbf{g}, \quad (2)$$

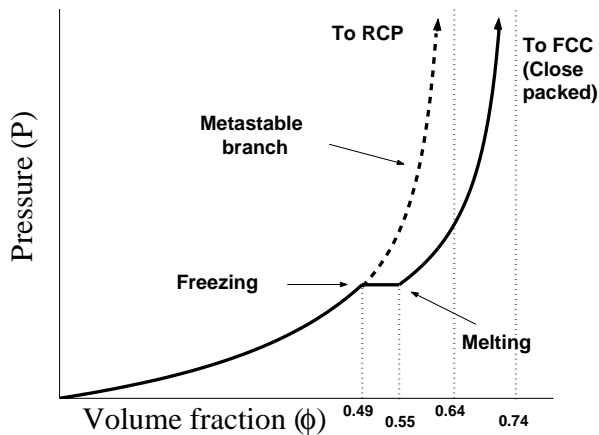


FIG. 1: Phase diagram of elastic hard sphere fluid, see text.

and the energy balance

$$\frac{3}{2} n \frac{dT}{dt} = -\nabla \cdot \mathbf{Q} + \mathbf{P} : \nabla \mathbf{v} - \Gamma, \quad (3)$$

where  $\Gamma$  is the energy loss rate due to the inelasticity of binary collisions. Here  $n(\mathbf{r}, t)$  is the number density of grains,  $T(\mathbf{r}, t)$  is the granular temperature,  $\mathbf{v}(\mathbf{r}, t)$  is the mean flow velocity,  $\mathbf{P}$  is the stress tensor,  $\mathbf{g}$  is the gravity acceleration,  $\mathbf{Q}$  is the heat flux, and  $d/dt = \partial/\partial t + \mathbf{v} \cdot \nabla$  is the total derivative. In the following we will put the particle mass to unity. The stress tensor  $\mathbf{P}$  can be written as

$$\mathbf{P} = [-p(n, T) + \mu(n, T) \text{tr}(\mathbf{D})] \mathbf{I} + 2\eta(n, T) \hat{\mathbf{D}}, \quad (4)$$

where

$$\mathbf{D} = (1/2) [\nabla v + (\nabla v)^T] \quad (5)$$

is the rate of deformation tensor,

$$\hat{\mathbf{D}} = \mathbf{D} - \frac{1}{3} \text{tr}(\mathbf{D}) \mathbf{I} \quad (6)$$

is the deviatoric part of  $\mathbf{D}$ , and  $\mathbf{I}$  is the identity tensor. We assume that the heat flux  $\mathbf{Q}$  is given by the Fourier law

$$\mathbf{Q} = -\kappa(n, T) \nabla T. \quad (7)$$

Similarly to dilute [13] and moderately dense [14] rapid granular flows, there can be an additional term in Eq. (7), proportional to the *density* gradient. This term must vanish as  $r \rightarrow 1$ , and it can be neglected in the nearly elastic limit  $q \ll 1$  that we are interested in throughout this paper.

To make the formulation complete, one needs constitutive relations: the equation of state  $p = p(n, T)$  and the dependences of the transport coefficients  $\mu$ ,  $\eta$  and  $\kappa$ , and of the energy loss rate  $\Gamma$  on  $n$  and  $T$ . For small and moderate densities, these relations can be derived from the Boltzmann or Enskog equation, properly generalized to

account for inelastic collisions [2, 3]. For very large densities, that we are interested in, one can use free volume arguments [15]. The resulting equation of state is

$$p = p_1 \frac{n_c^2 T}{n_c - n}, \quad (8)$$

where  $n_c = \sqrt{2}/d^3$  is the particle number density at close packing, and  $p_1$  is a numerical factor of order unity. Here and in the following we will write  $n_c$  instead of  $n_{fcc}$  (face-centered cubic). The temperature dependence in Eq. (8) is exact. We assume that all transport coefficients (except for the shear viscosity  $\eta$ , see below), diverge like  $(n_c - n)^{-1}$  near the close packing density [9]. Therefore, one can write the bulk viscosity coefficient  $\mu(n, T)$ , the thermal conductivity  $\kappa(n, T)$ , and the energy loss rate  $\Gamma(n, T)$  in the following form

$$\begin{aligned} \mu &= \mu_1 \frac{n_c T^{1/2}}{(n_c - n) d^2}, \\ \kappa &= \kappa_1 \frac{n_c T^{1/2}}{(n_c - n) d^2}, \\ \Gamma &= \Gamma_1 (1 - r^2) \frac{n_c^2 T^{3/2}}{(n_c - n) d}. \end{aligned} \quad (9)$$

Equations (9) are valid in the limit  $n_c - n \ll n_c$ . The temperature dependences are exact. The numerical factors  $\mu_1$ ,  $\kappa_1$ , and  $\Gamma_1$  are of order unity and presently unknown; they can be found in MD simulations. The same type of divergence of the transport coefficients (again, except for the coefficient of shear viscosity  $\eta$ ) was assumed in Ref. [10], but in the vicinity of the *random* close packing density.

There is a recent evidence in the literature that the shear viscosity coefficient  $\eta$  of elastic hard disk fluid grows faster with the density, at high densities, than the rest of the transport coefficients [16]. We believe that this behavior remains qualitatively correct also for three dimensional systems. Bocquet *et al.* [10] accounted for this fact in their description of the plane shear flow near the random close packing density. They proposed, by analogy with the behavior of supercooled liquids above the glass transition, that the shear viscosity coefficient diverges at random close packing density, but with a larger exponent:  $\eta \sim (n_{rcp} - n)^{-\beta}$ ,  $\beta > 1$ . In our model of a crystallized shear flow we suggest a different approach. We will accommodate a recent finding of Luding *et al.* [16] that the shear viscosity coefficient diverges like  $(n_c^* - n)^{-1}$  at a density  $n_c^* < n_c$ :

$$\eta = \eta_1 \frac{n_c T^{1/2}}{(n_c^* - n) d^2}, \quad (10)$$

where  $\eta_1$  is a numerical factor of order unity, which is presently unknown. Divergence of the shear viscosity implies that the fluid is jammed on a *macroscopic* length scale. While a shear flow in a macroscopically jammed system is impossible, the system of hard spheres may still

have finite temperature, pressure, heat conduction, and collisional energy loss.

There are arguments in the literature (see, *e.g.*, Santos *et al.* [17]) that steady sheared states of granular fluids are intrinsically non-Newtonian (that is, require a description beyond Navier-Stokes order). Why are such effects not included in our description? The reason is that non-Newtonian effects arise when one treats the inelasticity of particle collisions in a non-perturbative way (postulating that the Boltzmann equation, generalized to inelastic collisions, remains applicable for finite inelasticity). In this paper we work in the limit of nearly elastic particle collisions. In the first order in the inelasticity one does not need to take into account any inelasticity corrections to the transport coefficients (for example, to the shear viscosity). The only place where the inelasticity enters in this leading-order theory is the inelastic loss term  $\Gamma$  in the energy equation (3).

### III. STEADY SHEAR FLOW CLOSE TO CRYSTALLIZATION

Now let us introduce the flow setting we will be dealing with in the rest of the paper. We consider a plane Couette geometry. The model system is infinite in the horizontal ( $x$ ) direction and driven by the upper wall  $y = H$  that moves horizontally with velocity  $u_0$ . The lower wall  $y = 0$  is at rest (of course, in the absence of gravity the upper and lower walls are interchangeable). The height  $H$  of the layer in this setting is not fixed. Instead, the upper wall is maintained at a constant pressure  $P_0$ , like in a recent experiment by Gollub's group [5]. As already mentioned above, we assume a very dense flow, so that the volume fraction is close *everywhere* to that of close packing:  $\phi_{fcc} - \phi \ll \phi_{fcc}$ .

As we consider a steady horizontal motion, the number density  $n$ , the granular temperature  $T$  and the horizontal velocity  $u$  depend only on the vertical coordinate  $y$ . Then it follows from the  $y$ -component of the momentum equation (2) that the pressure is constant throughout the system:

$$p(y) = P_0. \quad (11)$$

Now we write down the  $x$ -component of the momentum equation (2) and rewrite the energy balance equation (3):

$$\begin{aligned} \frac{d}{dy} \left( \eta \frac{du}{dy} \right) &= 0, \\ \frac{d}{dy} \left( \kappa \frac{dT}{dy} \right) + \eta \left( \frac{du}{dy} \right)^2 - \Gamma(n, T) &= 0, \end{aligned} \quad (12)$$

where the constitutive relations are given by Eqs. (8)-(10). Equations (8)-(12) must be complemented by boundary conditions. We will assume rough walls and no-slip boundary conditions for the horizontal velocity:  $u(y = 0) = 0$ ,  $u(y = H) = u_0$ . The problem of evaluation of the granular heat flux at the rough walls was

addressed by Chou [18]. He considered a model where inelastic spheres were driven by walls with attached half-spheres (bumpy walls.) Extending an earlier treatment by Richman [19], Chou calculated the heat flux and the slip velocity at the boundaries. He showed that the heat flux at the boundaries can be positive or negative, depending on whether the "slip work" is larger or smaller than the energy loss due to inelastic particle collisions with the walls. For some values of parameters the total heat flux to the boundaries vanishes [18]. For simplicity, we will assume a vanishing heat flux and therefore prescribe  $dT/dy(y = 0) = dT/dy(y = H) = 0$ . The total number of particles is conserved, which yields a normalization condition for the density:  $\int_0^H n(y) dy = N$ , where  $N$  is the number of particles per unit area in the  $xz$  plane.

Let us rescale the vertical coordinate  $y$  by the (*a priori* unknown) system height  $H$ , the horizontal velocity  $u$  by the upper plate velocity  $u_0$ , the density  $n$  by the close-packing density  $n_c$ , and the temperature  $T$  by the ratio  $P_0/n_c$  of the constant applied pressure and close-packing density. Rewriting the equations in the scaled form, we obtain

$$\begin{aligned} p_1 \frac{T}{1-n} &= 1, \\ \frac{d}{dy} \left( \frac{T^{1/2}}{1-\lambda-n} \frac{du}{dy} \right) &= 0, \\ \frac{d}{dy} \left( \frac{T^{1/2}}{1-n} \frac{dT}{dy} \right) + \\ \frac{\eta_1}{\kappa_1} \frac{MT^{1/2}}{1-\lambda-n} \left( \frac{du}{dy} \right)^2 - \frac{\Gamma_1}{\kappa_1} \frac{2RT^{3/2}}{1-n} &= 0, \end{aligned} \quad (13)$$

where  $M = n_c u_0^2 / P_0$  is the square of the effective Mach number of the flow, and  $\lambda = 1 - n_c^* / n_c$  is a small positive numerical factor. For simplicity, the three presently unknown constants  $p_1 = \mathcal{O}(1)$ ,  $\eta_1 / \kappa_1 = \mathcal{O}(1)$  and  $\Gamma_1 / \kappa_1 = \mathcal{O}(1)$  are taken to be unity in the following. As the system height is unknown *a priori*, the scaled quantity  $R = (1 - r^2) H^2 / (2d^2)$  must be determined from the solution of the problem. From the first of Eqs. (13) we find a simple relation between the scaled density and temperature:  $T(y) = 1 - n(y)$ . Then, introducing a convenient auxiliary variable  $\epsilon(y) = [1 - n(y)]^{1/2} \ll 1$ , we rewrite the remaining Eqs. (13) as

$$\begin{aligned} \frac{du}{dy} &= \sqrt{\frac{2c}{M}} \frac{\epsilon^2 - \lambda}{\epsilon}, \\ \frac{d^2 \epsilon}{dy^2} + (c - R) \epsilon - \frac{c \lambda}{\epsilon} &= 0, \end{aligned} \quad (14)$$

where  $c$  is an unknown constant to be found from the solution of the problem. The boundary and normalization conditions are

$$u(y = 0) = 0, \quad u(y = 1) = 1,$$

$$\frac{d\epsilon}{dy}(y=0) = \frac{d\epsilon}{dy}(y=1) = 0, \quad (16)$$

$$\int_0^1 [1 - \epsilon(y)^2] dy = \frac{f}{R^{1/2}},$$

where  $f = (1 - r^2)^{1/2} N d^2 / 2$ . The steady flow equations (14)-(16) include two (known) scaled parameters:  $M$  and  $f$ . There are five unknown parameters in the problem:  $c$ ,  $R$  and three arbitrary constants which determine the solutions of the ordinary differential equations (14) and (15) for  $u(y)$  and  $\epsilon(y)$ , respectively. Correspondingly, there are five conditions (16) to determine the unknown parameters. In the following, when solving the equations numerically, we put  $\lambda = 0.05$ .

Before we get into a detailed description of the steady flow solutions of Eqs. (14)-(16), here is an overview of the results. Strikingly, there is an infinite number of steady flow solutions. They all can be parameterized by *three* parameters: the scaled numbers  $M$  and  $f$  and an integer number  $m = 1, 2, \dots$ . For a fixed  $m$ , there are three possible types of solutions in different regions of the phase diagram  $(M, f)$ , see Fig. 2. The simplest solution is the uniform, or linear shear flow that exists for any values of  $M$  and  $f$ . Here the velocity gradient, density and temperature are all constant. In region B (between the solid and dashed lines of Fig. 2), there is an additional one-phase solution: the one with nonlinear profiles of density, temperature and velocity. Finally, there is a multi-layer two-phase solution which exists in regions A and B, that is below the dashed line. The flow there is organized in several distinct layers. In the ‘‘solid-phase’’ layers the density is larger than the critical density  $n_c^*$  at which the shear viscosity diverges. Therefore, these layers move as a whole with a velocity  $u = \text{const}$ , while the temperature and density profiles are non-trivial. In the ‘‘fluid phase’’ layers there is a mean flow with non-trivial profiles of the velocity, temperature and density. The density, temperature, heat flux and velocity are continuous at the interface between the layers. This means in particular, that there is no macroscopic flow in the bottom layer of the granulate, and the inelastic energy losses there are balanced by the conduction of heat from the (flowing) top layer.

Now let us consider these solutions in more detail. We start with the simplest one: the uniform shear flow. Here  $\epsilon$  is independent of  $y$ , and Eq. (15) yields

$$\epsilon = \sqrt{\frac{c\lambda}{c-R}}.$$

Substituting this value into Eq. (14) and integrating in  $y$ , we obtain a linear velocity profile

$$u(y) = R \sqrt{\frac{2\lambda}{M(c-R)}} y. \quad (17)$$

Using the normalization condition and the condition

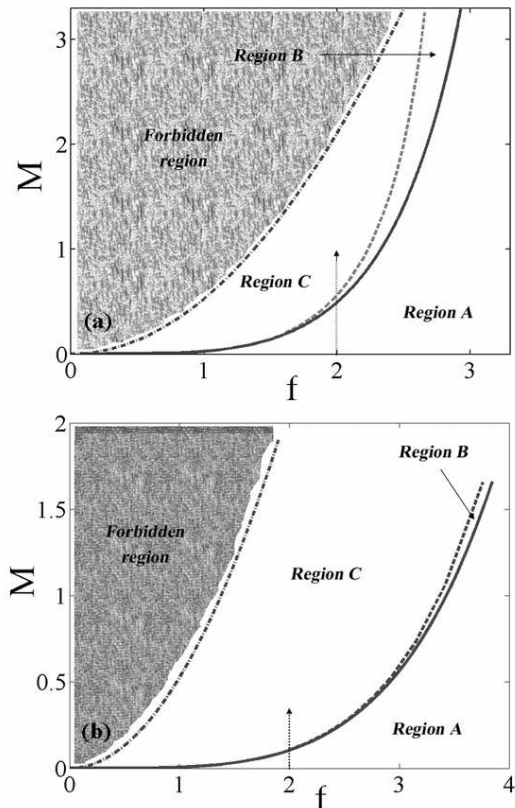


FIG. 2: Hydrodynamic phase diagram of the steady flow solutions for  $m = 1$  (the upper panel) and  $m = 2$  (the lower panel) in terms of the scaled parameters  $f$  and  $M$ . In the regions A there are: a multi-layer flow and an (unstable) uniform flow. In the regions B there are: a multi-layer flow, a non-uniform flow and an (unstable) uniform flow. In the regions C there is only a (stable) uniform flow. In the forbidden regions the granulate is not dense enough for our theory to be valid. Plausible bifurcation diagrams, corresponding to the dotted arrows  $f = 2$ , are shown, for the cases of  $m = 1$  and  $m = 2$  in Fig. 7.

$u(y=1) = 1$ , we obtain

$$1 - \frac{c\lambda}{c-R} = \frac{f}{\sqrt{R}} \quad \text{and} \quad c = R + \frac{2\lambda R^2}{M}. \quad (18)$$

Solving these two algebraic equations, we calculate  $R$

$$R = \frac{f^2}{2(1-\lambda)^2} \times \left[ 1 + \frac{M(1-\lambda)}{f^2} + \left( 1 + \frac{2M(1-\lambda)}{f^2} \right)^{1/2} \right] \quad (19)$$

and obtain the scaled velocity profile and the constant value of  $\epsilon$ :

$$u_0(y) = y, \quad \epsilon = \epsilon_* = \left[ \lambda + \frac{(1-\lambda)k_1}{1+k_1+(1+2k_1)^{1/2}} \right]^{1/2}, \quad (20)$$

where  $k_1 = M(1 - \lambda)f^{-2}$ . Notice that  $\epsilon_*$  always satisfies the condition  $\epsilon > \lambda^{1/2}$  or, in the original variables,  $n < n_c^*$ : the density of the uniform flow is smaller than the critical density at which the shear viscosity diverges. Note also that although the uniform shear flow solution [Eq. (20)] formally exists everywhere, the assumption  $\epsilon \ll 1$  demands  $k_1 \ll 1$ . Therefore, the solution is valid for  $M \ll f^2/(1 - \lambda)$ . This inequality breaks down in the forbidden regions of the phase diagram, see Fig. 2.

The nonlinear solution, which exists in region B, can be found numerically. We used the following numerical procedure, realized in Matlab. Let us denote  $\epsilon_0 \equiv \epsilon(y = 0)$ . For fixed  $R$  and  $f$ , we first solve Eq. (15) by varying parameters  $\epsilon_0$  and  $c$  and demanding  $d\epsilon/dy(y = 1) = 0$  and the normalization condition. This procedure yields  $\epsilon(y)$ . Then we solve Eq. (14) and find the velocity profile  $u(y)$  and the corresponding value of parameter  $M$  from the condition  $u(y = 1) = 1$ .

An important insight into the nature of this solution is provided by a mechanical analogy following from Eq. (15). Let  $\epsilon$  be a ‘‘coordinate’’, while the vertical coordinate  $y$  be ‘‘time’’. Then Eq. (15) describes a Newtonian particle oscillating in the potential well  $U(\epsilon) = (1/2)(c - R)\epsilon^2 - c\lambda \ln \epsilon$ . The boundary conditions select a family of solutions. A typical solution includes an integer number  $m$  of halves of the oscillation period, and a completion of these oscillations takes the system a unit ‘‘time’’,  $m\tau/2 = 1$  [see Eq. (21)], where  $\tau$  is the oscillation period. Figure 3 shows an example of particle in the potential well, while the resulting spatial profiles of  $\epsilon(y)$ ,  $u(y)$  and  $n(y)$  for a one-half of a full oscillation ( $m = 1$ ), and for a full oscillation ( $m = 2$ ), are shown in Fig. 4.

At a fixed  $m$ , this solution exists in region B of the phase plane of parameters  $f$  and  $M$ . This region is limited by two curves  $M = M(f)$  (see Fig. 2). The first curve is obtained as one approaches the bottom of the potential well. Here the oscillation amplitude (that is, the density contrast in the system) vanishes. Expanding the potential  $U(\epsilon)$  near the bottom of the potential well  $\epsilon = [c\lambda/(c - R)]^{1/2}$ , we can calculate the oscillation period  $\tau$ :

$$\tau = \frac{2}{m} = \pi \left( \frac{2}{c - R} \right)^{1/2}. \quad (21)$$

The bottom of the well corresponds to a uniform shear flow, but Eq. (21) must be obeyed arbitrarily close to the bottom of the well. Using Eq. (21) and the second equation of Eqs. (18), we obtain  $R = (m\pi/2)(M/\lambda)^{1/2}$  and  $c = R + m^2\pi^2/2$ . Substituting it into the first equation of Eqs. (18), we obtain the lower boundary of region B in terms of  $f$  and  $M$ :

$$f = \left( \frac{m\pi}{2} \right)^{1/2} \left( \frac{M}{\lambda} \right)^{1/4} \left[ 1 - \lambda - \frac{(\lambda M)^{1/2}}{m\pi} \right]. \quad (22)$$

For  $m = 1$  and  $m = 2$  these curves are shown by the solid lines in Fig. 2. They determine the boundary between the regions A and B for each  $m$ .

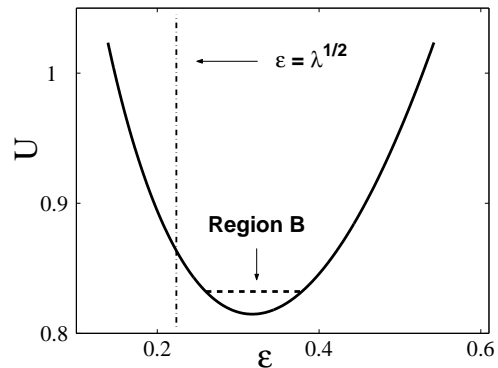


FIG. 3: The mechanical analogy for Eq. (15). Shown is a trajectory (the dashed line) of a classical particle in the potential well  $U(\epsilon)$  (the solid line, see text) which corresponds to regions B in Fig. 2. See Figure 4 for the resulting spatial profiles, which correspond to a one-half of the oscillation ( $m = 1$ ) and a full oscillation ( $m = 2$ , here the potential changes as the parameter  $M$  is different.) The oscillating solutions exist only inside the potential well, and only for  $\epsilon(y = 0) > \lambda^{1/2}$ , when the density is everywhere below the critical density at which the shear viscosity diverges. The parameters for this figure are  $M = 0.5158$  and  $f = 2$ .

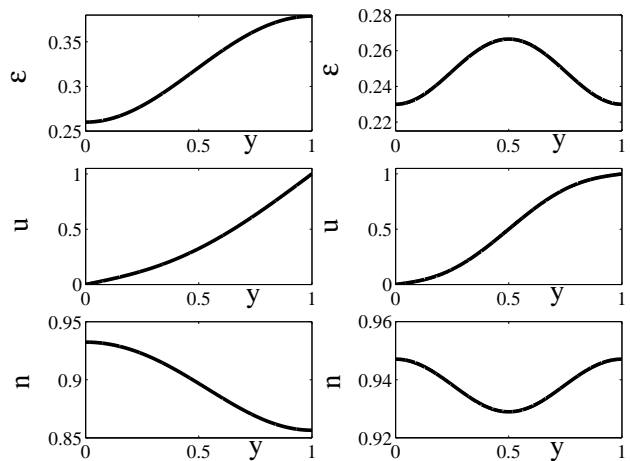


FIG. 4: The profiles of  $\epsilon(y) = [1 - n(y)]^{1/2}$  (the upper row), the scaled velocity  $u(y)$  (the middle row), and the scaled density  $n(y)$  (the bottom row), which correspond to region B in Figure 2. The profiles in the left column (respectively, in the right column) correspond to  $m = 1$ , a one-half of a full oscillation (respectively, to  $m = 2$ , a full oscillation) in the potential well, see Fig. 3. The parameters are  $f = 2$  and  $M = 0.5158$  (the left column), and  $f = 2$  and  $M = 0.1050$  (the right column).

The second limiting curve (plotted by the dashed lines in Fig. 2 for  $m = 1$  and  $m = 2$ ) is obtained numerically by putting  $\epsilon_0 = \lambda^{1/2}$  (see Fig. 3). This curve determines the boundary between the regions B and C.

Now let us consider the most interesting multi-layer two-phase family of solutions, parameterized by the same

number  $m \geq 1$  that now can be associated with the number of “solid” layers. Due to continuity of the velocity field, there is no macroscopic flow in the bottom layer of the granulate for any  $m$ , while the inelastic energy losses there are balanced by the heat conduction from the fluid-like top layer. A typical flow here consists of  $m$  zero-shear (solid-like) layers, each of which moving as a whole, separated by fluid-like regions. As we are dealing with a hard-sphere model, the granulate is fluidized within the “solid” layers: the granular temperature is non-zero, and there is energy flow through the boundaries of the layers. Let us first consider the  $m = 1$  solution. Here the only solid-like layer is at the bottom, and it is at rest. Putting  $c = 0$  in Eqs. (15) and (14) we obtain  $\epsilon(y) = \epsilon_0 \cosh(R^{1/2}y)$ . The height of the bottom layer is determined from the condition  $\epsilon(h) = \lambda^{1/2}$ . At the interface between the two layers we demand continuity of the density (and, therefore, of the temperature), of the heat flux, and of the velocity. Similarly to the procedure performed in region B, we solve the problem numerically by shooting in two parameters  $\epsilon_0$  and  $c$  (for the top layer) for fixed values of  $R$  and  $f$ , and then calculate the profiles and the respective value of the parameter  $M$ . Typical profiles  $\epsilon(y)$ ,  $u(y)$  and  $n(y)$  for  $m = 1$  are shown in Fig. 5, the left column. A multi-layer solution  $m > 1$  is obtained in a similar way, by demanding that the velocity in any solid layer is constant, while the density, temperature, heat flux and velocity are continuous at all interfaces between the layers. Typical profiles of  $\epsilon(y)$ ,  $u(y)$  and  $n(y)$  for  $m = 2$  are shown in Fig. 5, right panel.

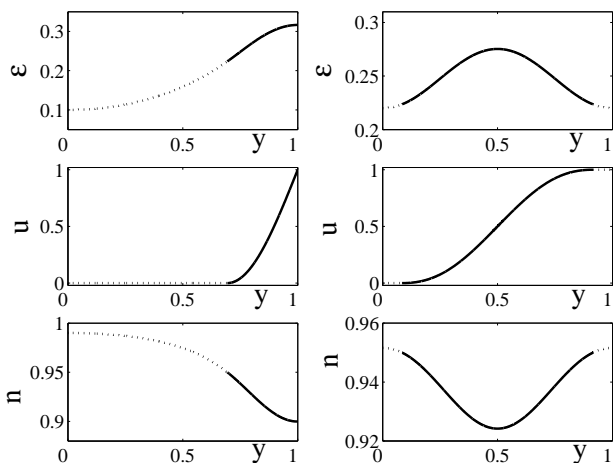


FIG. 5: The profiles of  $\epsilon(y)$  (the upper row), the velocity  $u(y)$  (the middle row) and the density  $n(y)$  (the bottom row) for the two-phase solution, for  $m = 1$  (the left column) and  $m = 2$  (the right column). The solutions for the fluid (solid) layers are shown by the solid (dotted) lines. The parameters are  $f = 2$  and  $M = 0.0492$  (the left column), and  $f = 2$  and  $M = 0.10148$  (the right column.)

At this point let us return, for a moment, to the case where the viscosity singularity is assumed to be at the same density  $n_c$  as the rest of transport coefficient. In

this case  $\lambda = 0$ , and the only possible solution is a uniform shear flow. Indeed, as  $\epsilon$  must be positive, the only acceptable solution of Eq. (15) with  $\lambda = 0$ , which obeys the no-flux boundary conditions, is  $\epsilon = \text{const}$  and  $c = R$ . Then the normalization condition [the last of Eqs. (16)] yields  $\epsilon^2 = 1 - f/R^{1/2}$ . One can obtain this solution directly by putting  $\lambda = 0$  in Eq. (20). Therefore, the assumption of a nonzero  $\lambda$  [the specific form of viscosity divergence, Eq. (10)], is crucial for the existence of non-trivial solutions.

One can see that, at fixed  $m$ , two different kinds of steady flow solutions exist in region A, for the same values of parameters  $M$  and  $f$ . Furthermore, three different kinds of steady flow solutions exist in region B, again for the same values of parameters  $M$  and  $f$  (see Fig. 2). What is the selection rule for these solutions? We give a partial answer to this question in the next section by performing a linear stability analysis of the uniform dense shear flow. Then we suggest plausible bifurcation diagrams of the system for different  $m$ .

#### IV. LINEAR STABILITY AND BIFURCATIONS

Our linear stability analysis of the uniform flow deals with the full set of (time-dependent) hydrodynamic equations (1)-(3) and constitutive relations (8)-(10). The details of linear stability analysis are shown in Appendix. Adding a small perturbations to the uniform shear flow and linearizing the equations, we finally arrive at a quadratic characteristic equation for the growth/damping rate  $\Gamma$  as a function of parameters and the wave number  $k$  [Eq. (A.4), see Appendix.] The two roots of this equation are real and correspond to two different collective modes of the system. One of them always decays. The other one is a purely growing mode for sufficiently small  $k$ , that is for long-wavelength perturbations. At small  $k$  we obtain:

$$\Gamma = \frac{2R^2 \lambda k^2}{ML \epsilon_* (M + fR^{1/2})} > 0, \quad (23)$$

where  $L = (2M)^{1/2} H/d$ . For sufficiently large  $k$ ,  $\Gamma$  is negative: the heat conduction suppresses the instability. The critical wave number for the instability is  $k_* = 2R\lambda^{1/2}/M^{1/2}$ . The dependence of the scaled growth rate  $\Gamma$  on the scaled wave number  $k$  is shown in Fig. 6.

Using Eq. (19), we obtain

$$k_* = \frac{f^2 \lambda^{1/2}}{2(1-\lambda)^2 M^{1/2}} \times \left[ 1 + \frac{M(1-\lambda)}{f^2} + \left( 1 + \frac{2M(1-\lambda)}{f^2} \right)^{1/2} \right]. \quad (24)$$

Notice that the time scale separation, employed here for the reduction of the order of the dispersion equation (see Appendix), breaks down when  $\epsilon_*$  approaches  $\lambda^{1/2}$ . As one can see from Eq. (20), this happens, for a fixed

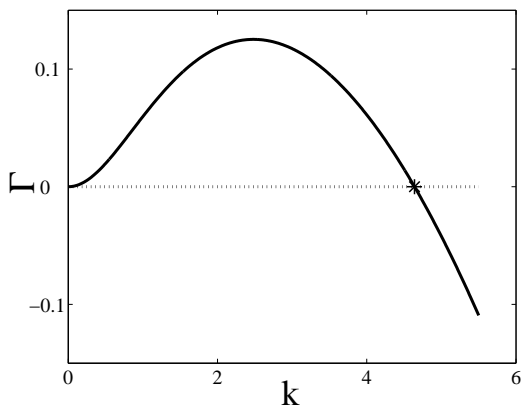


FIG. 6: The scaled growth rate  $\Gamma$ , calculated from Eq. (A.4), versus the scaled wave number  $k$ . The long-wavelength modes with  $k < k_*$  (the value of  $k_*$  is indicated by the asterisk) are unstable. The parameters  $f = 2$ ,  $M = 0.2$ ,  $\lambda = 0.05$ , and  $L = 100$  correspond to region *A* in Fig. 2a and to region *C* in Fig. 2b.

$f$ , when  $M$  becomes sufficiently small. Importantly, the final results (23) and (24) remain valid in the general case, as we obtained from the full, unreduced fourth-order dispersion equation for  $\Gamma(k)$ .

The wave number  $k$  of the perturbation is quantized by the boundary conditions. Indeed, the velocity perturbations must vanish at the upper and lower plates:  $u_1(y = 0, t) = u_1(y = 1, t) = v_1(y = 0, t) = v_1(y = 1, t) = 0$ . These conditions yield a discrete spectrum of wave numbers:  $k = \pi m$ , where  $m = 1, 2, 3, \dots$ . Therefore, the instability threshold is  $k_* = \pi$ . This equation determines a curve  $f(M)$  on the  $(f, M)$  plane. One can see that this curve coincides with the curve  $f(M)$  determined by Eq. (22) for  $m = 1$ : the borderline between regions *A* and *B* in Fig. 2. Similarly, the threshold for  $m = 2$  perturbation  $k_* = 2\pi$  coincides with the curve  $f(M)$  determined by Eq. (22) for  $m = 2$ , and so on. This is not entirely surprising: as the instability is aperiodic, its threshold is provided by the marginal stability condition. It is convenient to characterize each steady flow solution by the maximum density contrast it predicts. In terms of the auxiliary variable  $\epsilon$ , we can define  $\delta$  as the maximum change in  $\epsilon$  throughout the system [for  $m = 1$  this gives  $\delta \equiv \epsilon(y = 1) - \epsilon(y = 0)$ .] We can calculate  $\delta$  as a function of parameters  $f$  and  $M$  for each steady flow solution. Figure 7 shows all the resulting branches of the solution (for  $m = 1$  and  $m = 2$ ) for a fixed  $f$ , while  $M$  serves as a control parameter. Furthermore, there is an infinite number of bifurcation diagrams for multi-layer solutions (for all integers  $m > 1$ ), which can be computed in a similar way.

In order to determine the bifurcation diagram of the system at a fixed  $m$ , one needs to perform a linear stability analysis of each branch of the solution. Unfortunately, such an analysis is quite cumbersome for the so-

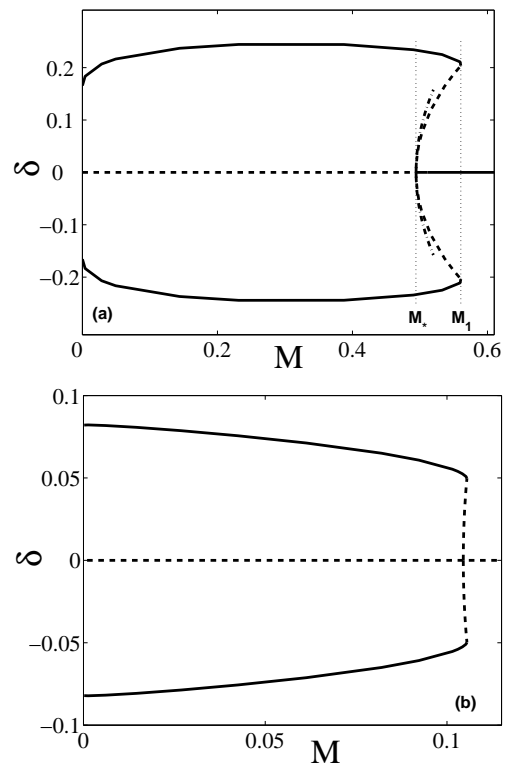


FIG. 7: A conjectured bifurcation diagrams of the steady flow for  $f = 2$  and  $\lambda = 0.05$ . Shown is the density contrast  $\delta$  versus  $M$  for different steady flow solutions for  $m = 1$  (the upper panel) and  $m = 2$  (the lower panel). The stable and unstable branches are indicated by the solid and dashed lines, respectively. We proved that the uniform flow ( $\delta = 0$ ) is unstable at  $M < M_*$ . The dash-dotted line in the upper panel is the asymptote of the branch bifurcating from the point  $M = M_*$ :  $\delta = 0.9856 \dots (M - M_*)^{1/2}$ .

lutions with  $\delta \neq 0$ . It is natural to assume that bifurcation, which occurs in the vicinity of the point  $M = M_*$ , at which the uniform shear flow (the one with  $\delta = 0$ ) changes from unstable [at  $M < M_*(f)$ ] to stable [at  $M > M_*(f)$ ], is an inverse pitchfork bifurcation. Based on this assumption, we obtain a simple bifurcation diagram, presented in Fig. 7. The stable solutions are indicated by solid lines, the unstable solutions by dashed lines. Let us consider the case of  $m = 1$  and follow the uniform shear flow solution (for which  $\delta = 0$ ) as  $M$  increases, starting from a small value, at fixed  $f$ . We pass from region *A* to region *B* of the hydrodynamic phase diagram (see the dotted arrow in Fig. 2) via an inverse pitchfork bifurcation. Here the uniform shear flow solution becomes stable, while the bifurcating “second solution” (the one with nonlinear density and velocity profiles) must be unstable. Exploiting the mechanical analogy (see Fig. 3), we can find the asymptote of the unstable branch in the close vicinity of the bifurcation point:  $\delta = A(f)(M - M_*)^{1/2}$ . Now let us move along the unstable branch  $\delta \neq 0$  and increase  $M$ . At some critical value of  $M$ , which depends on  $f$ , we reach the border be-



tween regions  $B$  and  $C$ . Here the unstable branch ends, as for larger  $M$  (region  $C$ ) the only possible solution is the uniform shear flow. There is, however, another solution which exists at smaller  $M$ . Figure 7 shows this *stable* branch which corresponds to the two-phase solution in regions  $A$  and  $B$  (see Fig. 2). This simple scenario predicts bistability at sufficiently small values of the parameter  $M$ , and a hysteresis on the interval  $[M_*(f), M_1(f)]$ , see Fig. 7. Note that the parameter  $L$  does not affect the bifurcation diagram, it only sets the time scales of transient motions in the system.

## V. SUMMARY AND DISCUSSION

We have considered here some aspects of shear-induced crystallization in a dense but rapid mono-disperse granular shear flow. We focused on a steady crystallized flow under a constant pressure and zero gravity. Assuming very high densities,  $n_c - n \ll n_c$ , we employed a version of the Navier-Stokes hydrodynamics for inelastic hard sphere fluid with *ad hoc* constitutive relations based on the free volume argument. In contrast to earlier works on rapid granular shear flow, we assumed that the shear viscosity coefficient  $\eta$  diverges at a density smaller than the close packing density  $n_c$ , while the rest of the constitutive relations diverge at  $n = n_c$ . We have determined the phase diagram of the steady flow in terms of three parameters: the effective Mach number, the scaled inelastic energy loss parameter, and an integer number  $m$ . In a steady flow the viscous heating of the granulate is balanced by energy dissipation through inelastic collisions. This balance is achieved, in different parts of the phase diagram, in different ways, producing either a uniform shear flow (with constant velocity gradient, density and temperature), or a flow with nonlinear velocity, density and temperature profiles. In some regions in the phase diagram two or three different steady flow solutions are possible for the same values of the parameters. We performed a linear stability analysis of the uniform flow, and suggested a plausible bifurcation diagram of the flow at a fixed  $m$ , which predicts bi-stability and hysteresis. We are unable as yet to find a selection principle that would prefer certain steady state solutions out of a multitude of solutions at different  $m$ . This non-trivial selection problem should be addressed in the future work.

One of the predictions of this work is the existence (and, we conjecture, stability) of two-phase solutions. The simplest solution of this type consists of a zero-shear (solid-like) layer at the bottom and a flowing top layer. Though there is no mean flow in the bottom layer, the particles there undergo “thermal” motion, and the granular temperature and pressure are non-zero. As a result, there is energy transfer through the bottom layer. There also exist two-phase multi-layer solutions, where solid-like layers, each of which moving as a whole, are separated by fluid-like regions with nonlinear velocity, density and temperature profiles. The existence of these

solutions is a direct consequence of our assumption that the coefficient of shear viscosity  $\eta$  in Eq. (10) diverges at a density which is smaller than the close packing density  $n_c$ .

A comparison of our results with those of Alam and coworkers is in order now. Alam *et al.* [20] investigated a plane Couette shear flow of inelastic hard sphere fluid, in a system with a fixed height, in a wide interval of densities: from the dilute limit to the random close packing density. They employed constitutive relations, all of which (including the viscosity) diverge at the random close packing density  $n_r$ . They found instability of the uniform shear flow when the inelasticity of the particle collisions becomes large enough or, alternatively, when the (fixed) system height exceeds a critical value for a fixed inelasticity. The uniform shear flow instability considered in our work is quite different: it *requires* viscosity divergence at a smaller density than the rest of constitutive relations. Indeed, Eqs. (22) and (24) show that this instability disappears when  $\lambda$  goes to zero. Although the parameter  $\lambda$  was identically zero in Ref. [20], instability was observed. Where does the difference come from? To remind the reader, the constitutive relations that we used assume a very dense system. Respectively, our results are valid only at leading order in the parameter  $(n_c - n)/n_c$ . We checked that, if one takes into account only the leading order terms in  $(n_r - n)/n_r$  in the equations of Alam *et al.* [20], the instability disappears.

Its worth mentioning that the steady flow equations (14)-(16) would not change if the crystal close packing density  $n_c$  were replaced by the random close packing density  $n_r$ . Such a formulation would follow from the assumption that the shear viscosity diverges at a density smaller than  $n_r$ . It would predict a variety of steady state solutions on the metastable branch, in the vicinity of the random close packing. We hope that the basic assumptions of our model (including the specific form of viscosity divergence) and its non-trivial predictions will be tested in MD simulations and in experiment on dense but *rapid* granular flow. Our work focused on a dense but rapid granular flow, assuming that the granulate is fully fluidized. In experiment it should be easier to achieve this regime when the shear is very large, so that the effective Mach number is of order unity (see Fig. 7.) Most experiments with dense granular flows are performed with slow flows, where the effective Mach number is small. For example, in the experiment of Gollub’s group [5] the parameter  $M$  was about  $5 \times 10^{-5}$ . In this regime the particles far from the moving boundary are in persistent contact with each other [5], inter-particle friction is important (see also [21]), and the model of inelastic hard spheres (and the Navier-Stokes hydrodynamics) is inapplicable.

In general, the model of inelastic hard sphere fluid is considered as a good approximation for dilute and moderately dense flows. Its validity range for dense flows is not well known [3]. Indeed, the particle collision rate increases with the density, so the assumption of instan-

taneous collisions, intrinsic in the model of hard spheres, may become restrictive at high densities. Being aware of this limitation, we still believe that the model of inelastic hard spheres can capture some of the physics of dense flow. Like in many other problems, it is useful to push this model to an extreme and analyze its predictions (some of which being quite unexpected as we have shown) in detail. We notice in passing that the two-phase flow predicted in this work resembles experimentally observed shear bands: localized regions of ordered granular flow, coexisting with essentially immobile solid-like regions [22].

The future experimental and theoretical work should elucidate the exact conditions under which shear-induced crystallization develops in granular flows. Though crystallization under shearing is well documented in MD simulations [7, 8], a recent experiment [23] showed that, under certain conditions, shearing can lead to *disorder*.

Finally, we did not attempt to describe in this work the shear-induced crystallization *process*. Such a description is beyond the reach of theory as of present. A promising approach to this problem should deal, in addition to the hydrodynamic fields, with an order parameter field and its dynamics. For slow granular flows such a description is now emerging [24].

### Acknowledgments

We acknowledge useful discussions with J.P. Gollub, S. Luding, P.V. Satorov, J.-C. Tsai, and A. Vilenkin. The work was supported by the the Israel Science Foundation (grant No. 107/05) and by the German-Israel Foundation for Scientific Research and Development (Grant I-795-166.10/2003).

### APPENDIX: DETAILS OF LINEAR STABILITY ANALYSIS

Let  $u$  and  $v$  be the velocity components in the  $x$  and  $y$  directions, respectively. We assume that the small perturbations to the uniform steady shear flow do not break the symmetry of the flow in the  $x$  and  $z$  directions:

$$\begin{aligned} n(y, t) &= n_0 + n_1(y, t), \\ T(y, t) &= T_0 + T_1(y, t), \\ u(y, t) &= u_0(y) + u_1(y, t), \\ v(y, t) &= v_1(y, t), \end{aligned} \quad (\text{A.1})$$

where index 0 denotes the uniform steady shear flow, see Eqs. (20), while  $T_0 = 1 - n_0 = \epsilon_*^2$ . Linearizing the hydrodynamic equations with respect to small perturbations, we arrive at

$$\frac{\partial n_1}{\partial t} + n_0 \frac{\partial v_1}{\partial y} = 0,$$

$$\begin{aligned} L n_0 \left( \frac{\partial u_1}{\partial t} + v_1 \frac{du_0}{dy} \right) &= \\ &= \frac{\partial}{\partial y} \left\{ \frac{T_0^{1/2}}{1 - \lambda - n_0} \left[ \frac{\partial u_1}{\partial y} + \left( \frac{T_1}{2T_0} + \frac{n_1}{1 - \lambda - n_0} \right) \frac{du_0}{dy} \right] \right\}, \\ L n_0 \frac{\partial v_1}{\partial t} &= -\frac{L}{M} \frac{\partial p_1}{\partial y} \\ &+ \frac{\partial}{\partial y} \left[ \left( \frac{T_0^{1/2}}{1 - n_0} + \frac{4T_0^{1/2}}{3(1 - \lambda - n_0)} \right) \frac{\partial v_1}{\partial y} \right], \\ \frac{3}{2} L n_0 \frac{\partial T_1}{\partial t} + L \frac{\partial v_1}{\partial y} &= \frac{\partial}{\partial y} \left( \frac{T_0^{1/2}}{1 - n_0} \frac{\partial T_1}{\partial y} \right) \\ &+ \frac{M T_0^{1/2}}{1 - \lambda - n_0} \frac{du_0}{dy} \left[ 2 \frac{\partial u_1}{\partial y} + \left( \frac{T_1}{2T_0} + \frac{n_1}{1 - \lambda - n_0} \right) \left( \frac{du_0}{dy} \right) \right] \\ &- \frac{2 R T_0^{3/2}}{1 - n_0} \left( \frac{3T_1}{2T_0} + \frac{n_1}{1 - n_0} \right), \end{aligned} \quad (\text{A.2})$$

where  $L = (2M)^{1/2} H/d$ , the time is measured in the units of  $H/u_0$ , and the value of  $H$  is determined by the unperturbed flow, that is by the uniform steady flow solution. One can check that the new parameter  $L$  (which is absent in the steady state problem, but enters the linear stability analysis), is fully determined by the scaled parameters  $f$  and  $M$  and by the restitution coefficient  $r$ .

A further simplification employs time scale separation. Let us compare the characteristic time scales of the problem. The acoustic time scale is  $\tau_1 = H \epsilon_* / (P_0/n_c)^{1/2}$ , the heat conduction time scale is  $\tau_2 = \tau_1 (H/d)$ , the energy loss time scale is  $\tau_3 = \tau_1 [H/(dR)]$ , and the viscous time is  $\tau_4 = \tau_1 (H/d) (\epsilon_*^2 - \lambda)/\epsilon_*^2$ . If the density is not too close to the density at which the shear viscosity diverges, that is if  $(H/d) (\epsilon_*^2 - \lambda)/\epsilon_*^2 \gg 1$ , one can separate the different time scales and eliminate the (acoustic-like) fast modes. This is equivalent to the assumption that the perturbations evolve in pressure equilibrium with the surroundings [25]. Using the condition  $\partial p_1/\partial t = 0$  instead of the full momentum equation [the third equation in Eqs. (A.2)], we obtain  $T_1 = -n_1$ . Then, differentiating the second equation of Eqs. (A.2) with respect to  $y$  and substituting  $\partial v_1/\partial y$  from the first equation of Eqs. (A.2), we arrive at

$$\begin{aligned} L (1 - \epsilon_*^2) \frac{\partial}{\partial t} \left( \frac{\partial u_1}{\partial y} - \frac{n_1}{1 - \epsilon_*^2} \right) &= \\ \frac{\partial^2}{\partial y^2} \left\{ \frac{\epsilon_*}{\epsilon_*^2 - \lambda} \left[ \frac{\partial u_1}{\partial y} + \left( -\frac{n_1}{2\epsilon_*^2} + \frac{n_1}{\epsilon_*^2 - \lambda} \right) \right] \right\}, \\ -L \frac{\partial n_1}{\partial t} \left[ \frac{3(1 - \epsilon_*^2)}{2} + \frac{1}{1 - \epsilon_*^2} \right] &= -\frac{\partial}{\partial y} \left( \frac{1}{\epsilon_*^2} \frac{\partial n_1}{\partial y} \right) + \\ \frac{M \epsilon_*}{\epsilon_*^2 - \lambda} \left[ 2 \frac{\partial u_1}{\partial y} + \left( -\frac{n_1}{2\epsilon_*^2} + \frac{n_1}{\epsilon_*^2 - \lambda} \right) \right] + \frac{R n_1}{\epsilon_*} &= 0, \end{aligned}$$

where we substituted  $du_0/dy = 1$  and  $T_0 = 1 - n_0 = \epsilon_*^2$ . Consider a single Fourier mode of the perturbation:

$$\begin{aligned} n_1(y, t) &= \tilde{n} \exp(\Gamma t + iky), \\ u_1(y, t) &= \tilde{u} \exp(\Gamma t + iky), \end{aligned}$$

where  $k$  is the wave number. Looking for nontrivial solutions, we obtain

$$\det(\mathbf{A}) = 0, \quad (\text{A.3})$$

where the elements of the matrix  $\mathbf{A}$  are

$$\begin{aligned} A_{11} &= -\Gamma L + \frac{4R^2 \epsilon_* k^2}{M^2} - \frac{Rk^2}{M \epsilon_*}, \\ A_{12} &= \frac{\Gamma L k f}{R^{1/2}} + \frac{2R \epsilon_* k^3}{M}, \\ A_{21} &= \Gamma L \left( \frac{3f}{2R^{1/2}} + \frac{R^{1/2}}{f} \right) + \frac{k^2}{\epsilon_*} + \frac{4R^2 \epsilon_*}{M}, \\ A_{22} &= 4Rk \epsilon_*. \end{aligned}$$

Equation (A.3) yields a quadratic equation for  $\Gamma$ :

$$a_2 \Gamma^2 + a_1 \Gamma + a_0 = 0, \quad (\text{A.4})$$

where the coefficients are

$$\begin{aligned} a_2 &= Lk^2 \left( 1 + \frac{3f^2}{2R} \right), \\ a_1 &= 4RLk \epsilon_* \left( 1 + \frac{fR^{1/2}}{M} \right) \\ &\quad + \frac{Lfk^3}{R^{1/2} \epsilon_*} \left( 1 + \frac{3R \epsilon_*^2}{M} + \frac{2R^2 \epsilon_*^2}{Mf^2} \right), \\ a_0 &= \frac{2Rk^3}{M} \left( k^2 - \frac{4R^2 \lambda}{M} \right). \end{aligned}$$

- 
- [1] *Challenges in Granular Physics*, edited by T.C. Halsey and A. Metha (World Scientific, Singapore, 2002).
- [2] J. T. Jenkins and M. W. Richman, *Phys. Fluids* **28**, 3485 (1985); *Arch. Ration. Mech. Anal.* **87**, 355 (1985).
- [3] C. S. Campbell, *Annu. Rev. Fluid Mech.* **22**, 57 (1990); I. Goldhirsch, *Annu. Rev. Fluid Mech.* **35**, 267 (2003).
- [4] M. Nicolas, P. Duru, and O. Pouliquen, *Eur. Phys. J. E* **3**, 309 (2000).
- [5] J.-C. Tsai, G. A. Voth, and J. P. Gollub, *Phys. Rev. Lett.* **91**, 064301 (2003); J.-C. Tsai and J. P. Gollub, *Phys. Rev. E* **70**, 031303 (2004); *ibid* **72**, 051304 (2005).
- [6] N. W. Mueggenburg, *Phys. Rev. E* **71**, 031301 (2005).
- [7] P. Zamankhan, T. Tynjala, W. Polashenski, P. Zamankhan, and P. Sarkomaa, *Phys. Rev. E* **60**, 7149 (1999).
- [8] M. Alam and S. Luding, *Phys. Fluids* **15**, 2298 (2003).
- [9] E.L. Grossman, T. Zhou, and E. Ben-Naim, *Phys. Rev. E* **55**, 4200 (1997).
- [10] L. Bocquet, W. Losert, D. Schalk, T. C. Lubensky, and J. P. Gollub, *Phys. Rev. E* **65**, 011307 (2002); L. Bocquet, J. Errami, and T. C. Lubensky, *Phys. Rev. Lett.* **89**, 184301 (2002).
- [11] B. Meerson, T. Pöschel, and Y. Bromberg, *Phys. Rev. Lett.* **91**, 024301 (2003).
- [12] M. D. Rintoul and S. Torquato, *J. Chem. Phys.* **105**, 9258 (1996); *Phys. Rev. Lett.* **77**, 4198 (1996); *Phys. Rev. E* **58**, 532 (1998); R. K. Bowles and R. J. Speedy, *Physica A* **262**, 76 (1999).
- [13] J.J. Brey, F. Moreno, and J.W. Dufty, *Phys. Rev. E* **54**, 445 (1996); N. Sela and I. Goldhirsch, *J. Fluid Mech.* **361**, 41 (1998); J.J. Brey, J.W. Dufty, C.S. Kim, and A. Santos, *Phys. Rev. E* **58**, 4638 (1998); R. Soto, M. Mareschal, and D. Risso, *Phys. Rev. Lett.* **83**, 5003 (1999).
- [14] J.F. Lutsko, *Phys. Rev. E* **72**, 021306 (2005).
- [15] Z.W. Salsburg and W.W. Wood, *J. Chem. Phys.* **37**, 798 (1962), and references therein.
- [16] R. Garcia-Rojo, S. Luding, and J. J. Brey, *cond-mat/0511671*.
- [17] A. Santos, V. Garzo, and J.W. Dufty, *Phys. Rev. E* **69**, 061303 (2004).
- [18] C.S. Chou, *Physica A* **287**, 127 (2000).
- [19] M.W. Richman, *Acta Mech.* **75**, 227 (1988).
- [20] M. Alam and P. R. Nott, *J. Fluid Mech* **377**, 99 (1998); M. Alam, V. H. Arakeri, P. R. Nott, J. D. Goddard, and H. J. Herrmann, *J. Fluid. Mech.* **523**, 277 (2005).
- [21] S.J. Moon, J.B. Swift, and H.L. Swinney, *Phys. Rev. E* **69**, 031301 (2004).
- [22] D.M. Mueth, G.F. Debregeas, G.S. Karczmar, P.J. Eng, S.R. Nagel, and H.M. Jaeger, *Nature* **406**, 385 (2000).
- [23] K.E. Daniels and R.P. Behringer, *Phys. Rev. Lett.* **94**, 168001 (2005).
- [24] D. Volfson, L.S. Tsimring, and I.S. Aranson, *Phys. Rev. Lett.* **90**, 254301 (2003); *Phys. Rev. E* **68**, 021301 (2003); *ibid* **69**, 031302 (2004).
- [25] B. Meerson, *Rev. Mod. Phys.* **68**, 215 (1996).